JOTCS A
Journal of the Turkish Chemical Society
Section: A
Chemistry
TURKISH CHEMICAL SOCIETY

The Influence of *Hibiscus tiliaceus* Leaf Extract as Capping Agent on the Zinc Oxide Properties and its Photo-simultaneous Performance

Riki Subagyo[1], Elfirza Zain[1], Siyam Martina[2,3], Saepurahman[2], Yuly Kusumawati[1,*]

[1]Department of Chemistry, Faculty of Science and Data Analytics, Institut Teknologi Sepuluh Nopember, Kampus ITS Keputih, 60111, Sukolilo, Surabaya, Indonesia
[2]Research Center for Chemistry, National Research and Innovation Agency (BRIN), Gd. 452 KST BJ Habibie, Serpong, Tangerang Selatan, Banten, 15314, Indonesia
[3]Department of Chemistry, Faculty of Mathematics and Natural Sciences, Universitas Negeri Semarang. Gd. D6 Kampus Sekaran Gunungpati, Semarang, 50229, Indonesia

Abstract: Polyol method, as one alternative in ZnO synthetic methods, have been developed and generated a nano-ZnO. However, the produced nano-ZnO is unstable due to its small particle size. To overcome the problems, we added *Hibiscus tiliaceus* leaves' extract during the ZnO (EZnO) synthesis to change the water content and hydrolysis ratio of Zn^{2+}/water. The addition of *H. tiliaceus* extract resulted in a shifting peak at (101) plane compared to ZnO synthesized without extract addition (WZnO). The use of *H. tiliaceus* extracts leads to the formation of large and non-uniform particles compared to the one prepared without the extract, which is in agreement with the intensity of diffraction pattern. The use of *H. tiliaceus* extracts shifted the bandgap energy to visible range. The performance of WZnO and EZnO samples was tested for simultaneous photo-oxidation of methylene blue and photo-reduction of Cr(VI) ions under UV-C irradiation. The EZnO is equally active as WZnO for Cr(VI) ion photo-reduction but less active for photo-oxidation of methylene blue. The presence of retained organic material in EZnO is plausibly affected by the adsorption and subsequent photo-oxidation of the bulky MB leading to a lower photo-oxidation performance. However, the activity of EZnO was a little bit lower than that of WZnO, revealing that the synergistic of particle size and band gap energy is a crucial factor in photo-removal process. In addition, the presence of phenolic compounds on the EZnO surface might change the nature properties of WZnO, which influence its performance.

Keywords: Zinc oxide, polyol, Hibiscus tiliaceus, Cr(VI), methylene blue, clean water

Submitted: October 8, 2023. **Accepted**: January 4, 2024.

Cite this: Subagyo R, Zain E, Martina S, Saepurahman, Kusumawati Y. The Influence of *Hibiscus tiliaceus* Leaf Extract as Capping Agent on the Zinc Oxide Properties and its Photo-simultaneous Performance. JOTCSA. 2024;11(2):547-556.

DOI: https://doi.org/10.18596/jotcsa.1372145

***Corresponding author.** E-mail: y_kusumawati@chem.its.ac.id

1. INTRODUCTION

Zinc oxide has been extensively utilized for pollutant photocatalysis due to its good properties, such as bandgap in UV region (3.2 eV), chemically stable, un-toxic, and cheap (1,2). The technique of synthesis of ZnO (i.e., polyol methods) has been developed in order to generate their size in nanoscale. ZnO nano-sized particles exhibit a high specific surface area, allowing fast reactions due to the high number of reaction sites (3,4). Nonetheless, ZnO nanoparticles are unstable due to their small particle size, which is attributed to their high surface energy. The high surface energy leads to particle agglomeration; regulating particle size, morphology, and microstructure becomes hard to observe. Particles' agglomeration was caused by sintering processes and Ostwald ripening (5). To overcome this issue, the stabilization of ZnO nano-sized particles has to be considered via particle immobilization on a supporting material or addition of capping agents (6–8).

Introducing capping agents (e.g., surfactants, polysaccharides, dendrimers, and polymers) during the ZnO synthesis has been observed and utilized due to the organic nature of the capping agent materials that serve on the ZnO nano-sized surface (9). Besides, the addition of capping agent also improves the compatibility of ZnO nano-sized with another phase or improves the functionalities (10). For instance, the influence of various capping agents has been studied in ZnO synthesis, including polyethylene glycol (PEG) and polyvinyl pyrrolidone (PVP) by coprecipitation method (11). The presence of PEG and PVP during the synthesis altered the crystallographic surface energy, promoting the anisotropic growth of nanosized ZnO. In order to minimize the utilization of chemicals as capping agents, plant extracts have been used due to their low cost and availability (12–14). *H. tiliaceus* is a tropical plant that has been used for various applications. The leaves' extracts of *H. tiliaceus* have been utilized for ZnO synthesis, as reported by Putri et al., showing good antioxidant activity (15). The compounds in the extract (including phenolic compounds) altered the formation of ZnO. The phenolic compound would act as a reduction agent and capping agent.

Here, we synthesized the ZnO using polyol methods. *H. tiliaceus* leaf extract was used to change the water contained in the polyol methods. The activity of the obtained ZnO (EZnO) was evaluated for simultaneous photo-oxidation of methylene blue and photo-reduction of chromium (Cr(VI)) ions under UV-C light irradiation. ZnO without *H. tiliaceus* extracts (WZnO) was also produced and utilized for simultaneous removal to compare their activities.

2. EXPERIMENTAL SECTION

2.1. Preparation of *Hibiscus tiliaceus* leaves extract

H. tiliaceus leaves were collected, washed using a water-ethanol solution, and dried in an oven set at 80 °C for three days until the leaves changed color from dark green to brown. The brown *H. tiliaceus* leaves were crushed using a blender and sieved to obtain a uniform size (100 mesh). The *H. tiliaceus* leaves' powder was mixed with aqua DM and stirred for 30 minutes at 70°C. The obtained filtrates were separated using centrifugation at 10000 rpm.

2.2. ZnO synthesis

The ZnO nanoparticles were synthesized using a polyol method utilizing a reflux system, as reported in ref. (1,16). $Zn(CH_3COO)_2{\cdot}H_2O$, NaOH, Aqua DM, and DEG were mixed at a mol ratio of 1:2:1. The reflux system was operated for one hour at 161°C. The obtained solids were separated using centrifugation at 10,000 rpm, followed by washing with ethanol and acetone. The obtained solid was then left for 3 days at 60 °C. The dried solid was collected and labeled as WZnO. In order to investigate the influence of *H. tiliaceus* leaf extract, the aqua DM was replaced with *H. tiliaceus* leaf extract. The obtained solid was labeled as EZnO.

2.3. Characterization

The WZnO and EZnO photocatalysts were characterized using several instruments to observe their characteristics. The structural properties of WZnO and EZnO photocatalysts were investigated using X-ray diffractometer (XRD, PAnalatical, 2θ = 5–90°), fourier transform infrared spectrophotometer (FTIR, Shimadzu, v = 4000–400 cm^{-1}), and field emission scanning electron microscope (FESEM, JEOL). Transmission electron microscope (TEM, Hitachi7700) was utilized to observe the nanostructure of WZnO. The optical properties of WZnO and EZnO were analyzed using ultraviolet-visible diffuse reflectance spectrophotometer (DR-UV-Vis, Agilent Cary 60, λ=200–800 nm).

2.4. Photocatalytic Activity Test

Photocatalytic activity of EZnO and WZnO was tested for simultaneous photo-oxidation of methylene blue and photo-reduction of Cr(VI) ions under UV-C irradiation. Briefly, 50 mg EznO or WZnO was dispersed in 12 mL Milli-Q water, followed by ultrasonication for 10 minutes. In a 300 mL crystallizing dish with a diameter of 9.5 cm, 18 mL of MB at 40 ppm and 20 mL of Cr(VI) ions at 40 ppm solutions were added, followed by the EZnO or WZnO dispersion. The final MB and Cr(VI) ions concentration was 14.4 and 16 ppm, respectively, and the [MB]/[Cr(VI)] ratio was 0.9. The crystallizing dish was put inside a 59.5 × 49.5 × 50 cm^3 UV-C chamber containing a Philips TUV 15W/G15 T8 lamp emitting a UV-C (λ = 254 nm) light. The dish was separated at 14.5 cm from the lamp. The dish was irradiated for 60 min and after that 2×1.5 mL of sample was taken, centrifuged at 7000 rpm for at least 10 min. 1 mL of clear solution was analyzed for its MB concentration by directly measuring its absorbance at 665 nm wavelength. Another 1 mL of clear solution was tested for its Cr(VI) ion concentration. The Cr(VI) ion concentration was determined colorimetrically by mixing 1 mL of the clear solution with 9 mL of MiliQ water, 200 µL of H_2SO_4 6N, and 1 mL of 1,5-diphenylcarbazide in acetone solution. The mixture was incubated for 10 min and the absorbance was measured at 540 nm wavelength using a Cary-60 UV-Vis spectrophotometer. To simulate MB and Cr(VI) ions removal due to adsorption, similar experiments for EZnO and WZnO were performed with the lamp turned off. An exact solution composition without photocatalysts was prepared and used as a reference. The percentage of removal is calculated as the difference between the absorbace of the solution after photo-oxidation or photo-reduction (A_t) and the absorbance of the reference (A_0) following Eq. 1.

$$\text{Removal efficiency (\%)} = 100 \times \frac{A_0 - A_t}{A_0} \qquad \text{Eq. 1}$$

The kinetic study of simultaneous photocatalytic of MB and Cr(VI) was performed in similar method by the variation of time irradiation. The addition of

scavenger agent was also performed as well as the preliminary test.

3. RESULTS AND DISCUSSION

The structural properties of EZnO and WZnO samples were investigated using XRD analysis and FTIR analysis. The diffraction pattern of EZnO and WZnO samples is shown in Figure 1 (a). All samples exhibit characteristic peaks of hexagonal wurtzite ZnO at 31.67, 34.39, 36.15, 47.57, 56.61, 62.81, 66.34, 67.88, 69.14, 72.49, and 76.92° which corresponded to (100), (002), (101), (102), (110), (103), (200), (112), (201), (004), and (202) planes, respectively. This result was similar to our previous study reported by Hosni et al. (16) and Zakiyah et al. (1). The intensity peaks of EZnO are higher than that of WZnO, indicating that *H. tiliaceus* leaves' extract increases the crystallinity of EZnO. The (101) plane has the highest intensity for all samples, implying that the ZnO samples grew strongly along the (101) direction, which reveals a high alignment degree along the c-axis and can be vital for tuning the aspect ratio. Figure 1 (b) showed an enlarged XRD peak of (101) plane showing a peak shift with the addition of *H. tiliaceus* leaves' extract, which was associated with the variant in residual strain developed in the crystal lattice. The strain induced shift along (101) direction might be a crucial factor in controlling the equatorial and axial growth of ZnO nanostructure. With the addition of *H. tiliaceus* leaves' extract, the (101) plane was slightly shifted to left compared to ZnO photocatalyst prepared without adding *H. tiliaceus* leaves' extract (WZnO). This suggests that c-axis growth is reduced by the addition of *H. tiliaceus* leaves' extract.

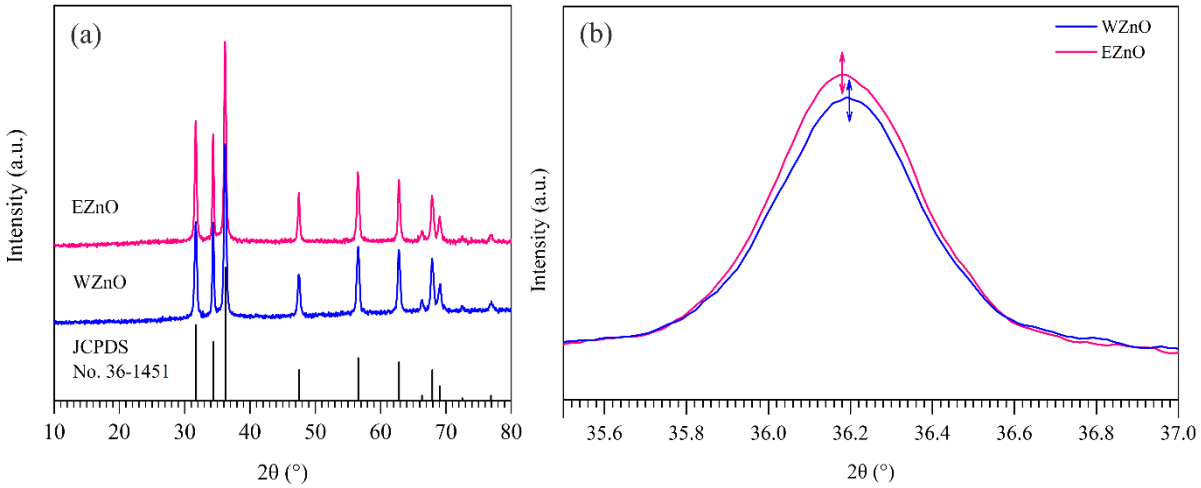

Figure 1: (a) diffraction pattern and (b) enlarged (101) peak of samples

FTIR analysis was carried out to analyze the presence of functional groups in WZnO and EZnO photocatalysts. Both WZnO and EZnO exhibit bands at 3430, 2922, 1564, 1407, and 500–400 cm^{-1} as shown in Figure 2. The band at 3430 cm^{-1} is attributed to the O–H (17), indicating the presence of physically adsorbed water. The band at 2922 cm^{-1} is attributed to the stretching vibration of –CH, confirming the presence of CH_2 and CH_3 groups (18). The absorption bands at 1564 and 1407 cm^{-1} are assigned to the symmetric and asymmetric stretching vibrations of C=O (19). The presence of bands at 2922, 1564, and 1407 cm^{-1} implies that both WZnO and EZnO contain organic material retained on their surface. The intensity of those bands is somewhat less pronounced in WZnO than in EZnO, suggesting that the EZnO retains more organic material than the WZnO. The organic compound in WZnO and EZnO is retained since the formation of ZnO did not use the calcination process. The presence of organic compounds might be correlated to the presence of DEG and flavonoid compounds extracted from *H. tiliaceus* leaves. The stretching vibration of Zn–O is observed at 500–400 cm^{-1}. In addition to the mentioned bands above, unlike WZnO, EZnO also exhibits prominent bands at 1300–1100 cm-1. These bands are likely due to the presence of other functional groups contributed by the *H. tiliaceus* leaf extract such as polyphenolic compounds adsorbed on the surface of EZnO via π-electron interaction of carbonyl group with the free orbital of Zn (20).

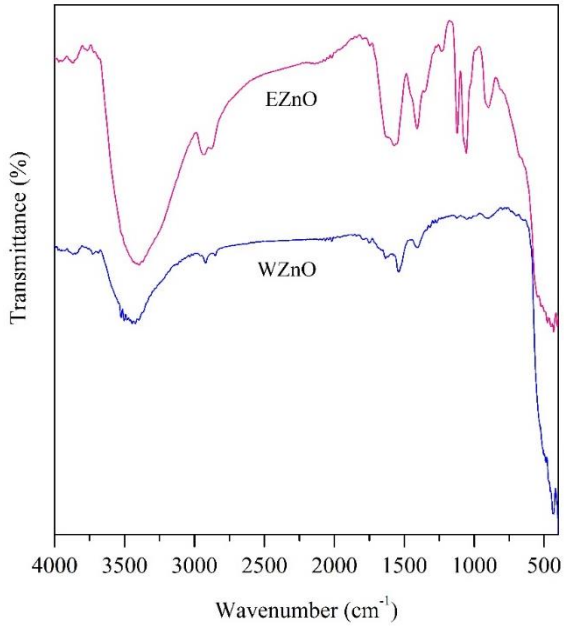

Figure 2: FTIR spectra of samples

The morphology of WZnO and EZnO photocatalysts is depicted in Figure 3. The WZnO photocatalysts formed a uniform nanosize rods-like morphology. The nanorods' morphology is a one-dimensional structure that enables a highly efficient charge carrier mobility due to decreased grain boundaries, disorder, discontinuous interface, and surface defects. In order to clarify the morphology of WZnO, TEM analysis has been carried out. As shown in Fig. 3b, it can be seen that the dominant morphology of WZnO is nanorods. However, several morphologies are also observed in WZnO, including hexagonal and sphere. The particle has a nano-size of 20 – 200 nm. Unlike the WZnO photocatalyst, the EZnO photocatalyst exhibits nanosize non-uniform morphology. It can be seen that adding the *H. tiliaceus* leaves' extract altered the ZnO formation, leading to the formation of non-uniform ZnO morphology. The difference is possibly due to the competitive interaction among DEG, *H. tiliaceus* leaf extract, and Zn^{2+} ions, which led to the formation of non-uniform structures.

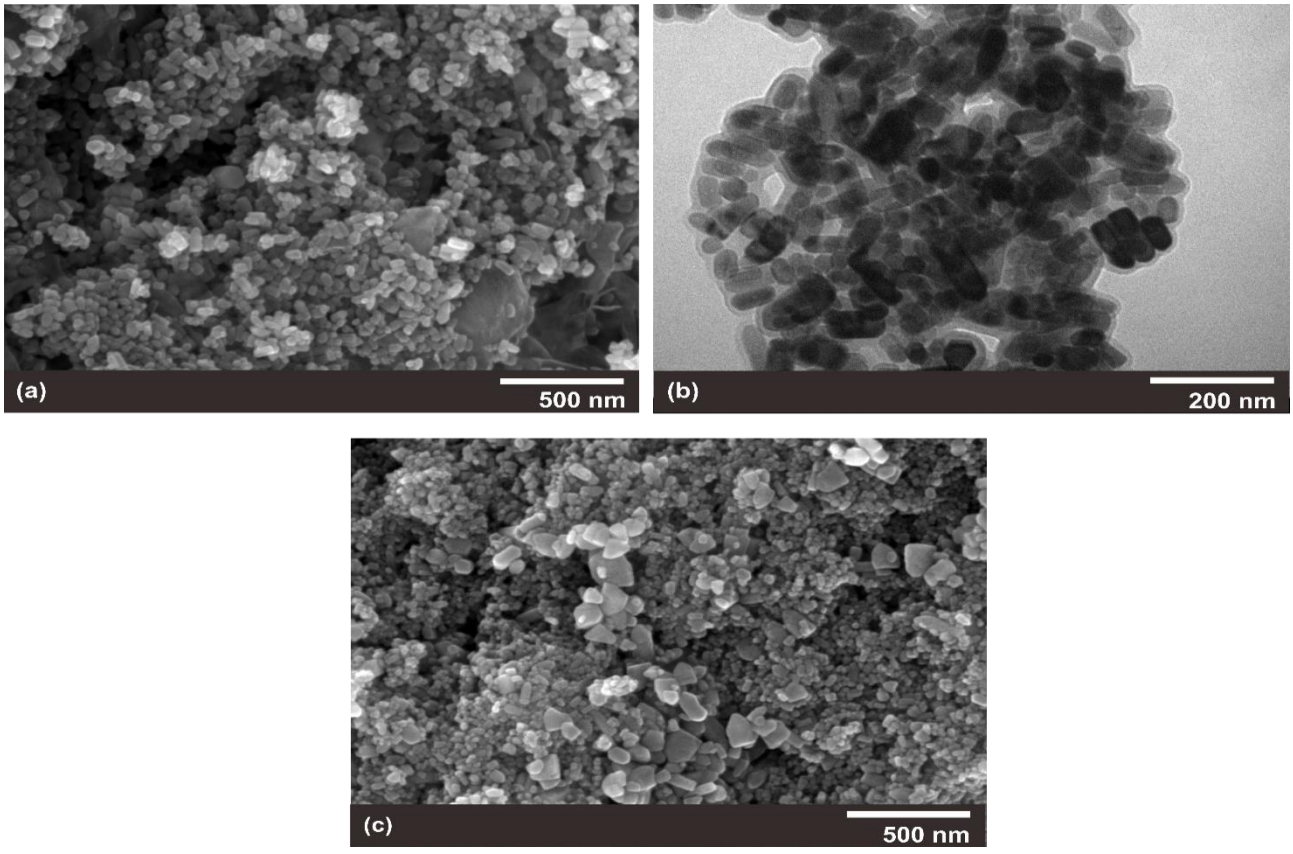

Figure 3: (a) FESEM and (b) TEM image of WZnO. (c) is FESEM image of EZnO

The optical properties of WZnO and EZnO photocatalysts were analyzed using UV-Vis DRS. The UV-Vis spectra of WZnO and EZnO are displayed in Figure 4. The WZnO exhibits a high absorption in UV region compared to the EZnO photocatalyst. The red shift in the absorption edge is observed after the addition of *H. tiliaceus* leaf extract, which is associated with bandgap-shifting. The band gap energies of WZnO and EZnO photocatayst were calculated using the Tauc plot following Eq. (2).

$$(\alpha h\nu)^{1/n} = A(h\nu - E_g) \qquad \text{Eq. (2)}$$

where A is a constant of proportionality, α is the photon absorption coefficient, $h\nu$ is the energy of photons, and E_g is the band gap energy. As shown in Figure 4b, the band gap energies of WZnO and EZnO are 3.18 eV and 3.05 eV, respectively. This result implies there was a red shift in the absorption edge. The red shift of the absorption edge is attributed to the position of the band level in the ZnO. The addition of *H. tiliaceus* leaf extract might have changed the position of the band level due to the presence of various organic compounds that affected the generation of EZnO. As a result, the band gap decreased.

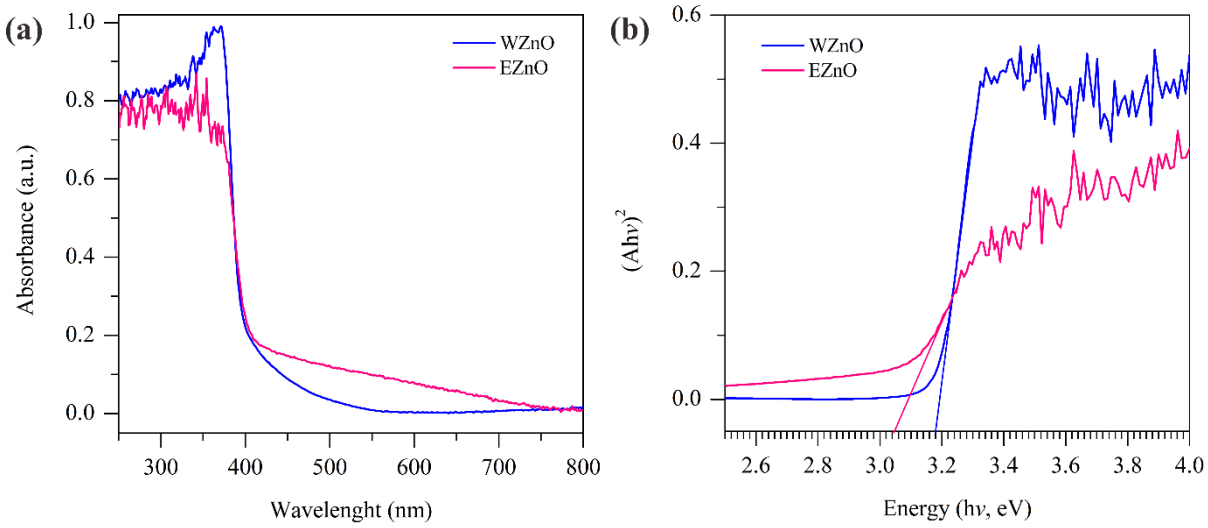

Figure 4: (a) Spectra UV-Vis and (b) Tauc plot of samples

The performance of the WZnO and EZnO photocatalysts in simultaneous photo-oxidation of MB and photo-reduction of Cr(VI) ions is illustrated in Figure 5. Dark experiments showed that the MB removal by the WZnO and EZnO photocatalysts is minor, implying that MB removal via adsorption is negligible (less than 4% after 60 min). The MB removal by WZnO photocatalyst was significantly increased under UV-C irradiation, where the MB removal reached 33.45% after only 10 min illumination and further increased to 72.30% after 60 min UV-C exposure (Figure 5 (left)). The MB removal by EZnO photocatalyst behaved similarly. However, the MB removal by the EZnO photocatalyst was slightly lower at 18.91 and 47.58% after 10- and 60-min UV-C illumination, respectively. This implies that the WZnO photocatalyst had better MB photo-oxidation performance than the EznO photocatalyst. The performance of the WZnO and EZnO photocatalysts for Cr(VI) ion photoreduction is shown in Figure 5 (right). The removal Cr(VI) ions in the dark was negligible (maximum was 6.60% after 60 min). The Cr(VI) ions' removal reached 20% after 10 min UV-C illumination and 63% after 60 min. Unlike the MB removal, there was no significant differences in the performance of the WZnO and EZnO photocatalysts for Cr(VI) ion photoreduction.

While the performance of WZnO and EZnO photocatalysts for MB photo-oxidation displayed a significant difference, their performance for Cr(VI) ion photoreduction exhibited no difference. This implies that the MB photo-oxidation is affected by the surface characteristics of the photocatalysts. As mentioned before, the EZnO sample contained more retained organic material as compared to the WZnO sample, as supported by the FTIR analyses. The presence of the organic material might have affected the bulky MB adsorption and subsequently photo-oxidation of MB, leading to a lower performance displayed by the EZnO. For Cr(VI) ion photoreduction, on the other hand, due to its smaller ionic diameter, the Cr(VI) ions might have no restriction to reach active sites in both WZnO and EZnO and underwent photo-reduction.

However, the efficiency of MB removal using EZnO is lower than that using WZnO. While the Cr (VI) removal using WZnO is slightly enhanced compares with what EZnO did. Compared with WZnO, EZnO particle size is smaller, reducing the active sites for dyes and leading to a decrease in photocatalytic performance, even though the band gap energy of EZnO is narrower than that of WZnO. It can be seen that the synergy of ZnO properties (nano-sized, surface area, band gap)

must be generated in order to obtain the optimum photocatalytic performance of ZnO. Nonetheless, the addition of *H. tiliaceus* leaves' extract to the ZnO synthesis can be a good candidate to alter the bandgap energy of ZnO in the visible region, with further development to achieve the synergistic nature of its properties for optimum activity performance.

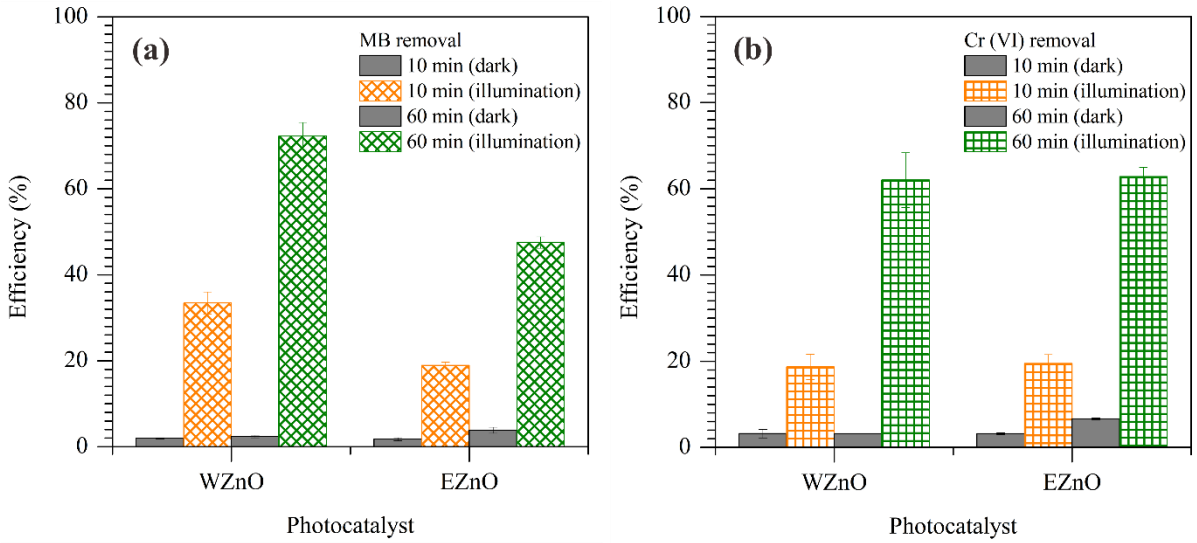

Figure 5: Simultaneous (a) photo-oxidation of MB efficiency and (b) photo-reduction efficiency of Cr (VI) ions by WZnO and EZnO photocatalysts under dark and illuminated conditions.

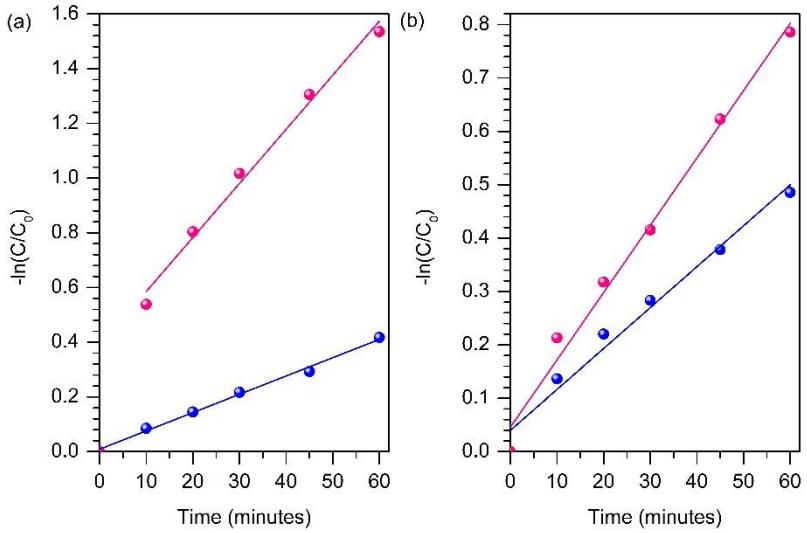

Figure 6: Kinetic study of simultaneous (a) photo-oxidation of MB efficiency and (b) photo-reduction efficiency of Cr (VI) ions by WZnO and EZnO photocatalysts.

Table 1: Summary of pseudo-first order kinetic of simultaneous photocatalytic of MB and Cr(VI)

Material	WZnO		EZnO	
	MB	Cr(VI)	MB	Cr(VI)
R^2	0.9868	0.9856	0.9936	0.9737
K_1 (min^{-1})	0.0198	0.0126	0.0067	0.0077
r (M min^{-1})	0.2851	0.2016	0.0965	0.1232

The kinetics of simultaneous photocatalytic reactions of Cr and MB have been determined by the pseudo-first order reaction. As shown in Figure 6, the kinetics of the simultaneous photocatalysis of Cr(VI) and MB are in agreement with the pseudo-first order. In the MB kinetic study, especially for WZnO, the kinetic study was plotted from 10 min to 60 min since the large improvement of MB removal from the initial to the 10 minutes correlated with the adsorption process of MB on the surface of WZnO. The pseudo-first order parameter was tabulated in Table 1. The reaction rate of WZnO is faster than that of EZnO. This result demonstrates that WZnO has a good ability to remove MB and Cr(VI). Besides, the MB reaction rate by WZnO is faster than the Cr(VI) reaction rate of WZnO, indicating that WZnO is more effective for MB photocatalysis. In contrast, the reaction rate of Cr(VI) by EZnO is faster compared to the reaction rate of MB by EZnO,

revealing that EZnO is suitable for photoreduction of Cr(VI). The presence of functional groups in organic compounds of *H.tiliaceus* leaves' extract might facilitate the photoreduction of Cr(VI) than the photooxidation of MB molecules. The K_1 value of WZnO and EZnO for Cr(VI) photoreduction is higher compared to the previous study using ZnO/graphene (21) and ZrO_2 (22), indicating that WZnO and EZnO have excellent ability to reduce Cr(VI) to Cr(III). However, the K_1 value of MB photooxidation is slightly low compared to previous studies using biosynthesis ZnO (23) and mesoporous ZnO (24). It can be due to the simultaneous photocatalytic process, leading to reaction competition between Cr(VI) and MB.

The mechanism of simultaneous photocatalysis of Cr(VI) and MB is proposed in Figure 7a. Upon light illumination, the electrons in the VB of ZnO are excited to the CB of ZnO. As a result, the equivalent number of holes was formed in the VB of ZnO. Both charge carriers diffused into the surface of ZnO, and a redox reaction took place. According to Butler and Ginley equation, the VB and CB levels of ZnO can be calculated following Eqs. (3) and (4) (25).

$$E_{VB} = X - E^e + \tfrac{1}{2}E_g \quad \text{Eq. (3)}$$

$$E_{CB} = E_{VB} - E_g \quad \text{Eq. (4)}$$

E_{VB}, E_{CB}, and E_g are the VB level, CB level, and band gap of ZnO. E^e and X are the free electron energy on hydrogen scale (4.5 eV) and the electronegativity of ZnO (5.79 eV). The calculated VB and CB levels of WZnO are 2.88 eV and -0.3 eV, respectively, whereas the VB and CB levels of EZnO are 2.82 eV and -0.24 eV, respectively.

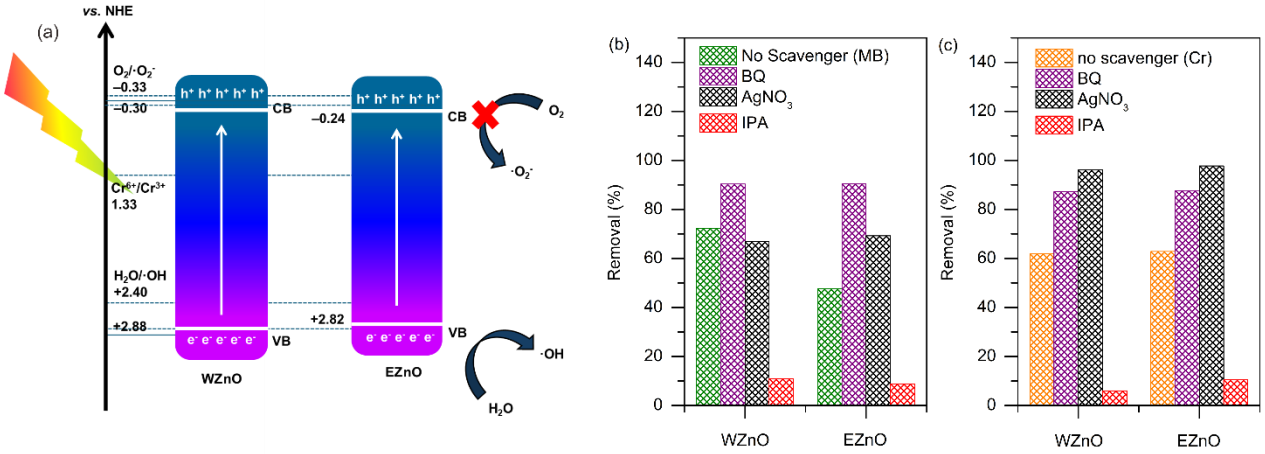

Figure 7: (a) Mechanism of photocatalytic by WznO and EZnO and (b, c) is the removal of MB and Cr(VI) after the addition of scavenger agent

The CB level of both ZnO is more negative compared to reduction potential of Cr(VI)/Cr(III) (E^0 = +1.33 eV *vs.* NHE), indicating that the photoreduction of Cr(VI) to Cr(III) is feasible. Besides, the VB level of both ZnO is more positive than that of oxidation potential of $OH^-/{\cdot}OH$ (E^0 = +2.40 eV *vs.* NHE), revealing that the oxidation reaction OH^- by h^+ easily occurred (24,26). However, the oxidation potential of $O_2/{\cdot}O_2^-$ (E^0 = –0.33 eV *vs.* NHE) is more negative compared to CB level of both ZnO, demonstrating that ${\cdot}O_2^-$ is impossible to generate. Since pH of the used Milli-Q water is under 7, the main species of Cr(VI) ions is $HCrO^{4-}$ or $Cr_2O_7^{2-}$ which require three and six electrons to reduce to Cr(III), respectively. Scavenger agents were added during the photocatalytic process to assess the presence of radical active species. The scavenger agents, including isopropanol (IPA), silver(I) nitrate ($AgNO_3$), and p-benzoquinone (BQ), were used to inhibit the activity of ·OH (27), e^- (28), and ${\cdot}O_2^-$ (29), respectively. As shown in Figure 7b and 7c, the addition of IPA decreased the photocatalytic activity of ZnO whereas adding BQ and $AgNO_3$ improved the photocatalytic activity. The improvement of photocatalytic activity by adding BQ and $AgNO_3$ might reveal that BQ and $AgNO_3$ can act as electron sinks. Specifically for $AgNO_3$, its presence during the irradiation can induce the formation of a Schottky junction, thereby enhancing electron transfer and facilitating the photoreduction process (30). Therefore, it can be noted that ·OH is an active species during the photocatalytic process.

4. CONCLUSION

H. tiliaceus leaves' extract influenced the properties of ZnO (EZnO). EZnO generated a crystalline structure and a large particle size compared with WZnO. Nevertheless, EZnO exhibited narrow bandgap energy in the visible region. However, the efficiency of MB removal using EZnO is lower than that using WZnO. While the Cr (VI) removal using EZnO is slightly reduced compared with WZnO. The synergy of ZnO properties (nano-sized, surface area, band gap) must be generated in order to obtain the optimum photocatalytic performance of ZnO. Nonetheless, the addition of *H. tiliaceus* leaves' extract in the ZnO synthesis can be a good candidate to alter bandgap energy of ZnO in the visible region, with

further development to achieve the synergistic nature of its properties for optimum activity performance.

5. CONFLICT OF INTEREST

There is no conflict of interest.

6. ACKNOWLEDGMENTS

The authors gratefully acknowledge financial support from the Institut Teknologi Sepuluh Nopember for this work, under the project scheme of the Publication Writing and IPR Incentive Program (PPHKI) 2024.

7. REFERENCES

1. Zakiyah A, Anindika GR, Kusumawati Y. Synthesis of zinc oxide (ZnO) nanoparticles by polyol method and its application on photocatalytic reduction of paracetamol concentration. AIP Conf Proc. 2021;2349.

2. Subagyo R, Kusumawati Y, Widayatno WB. Kinetic study of methylene blue photocatalytic decolorization using zinc oxide under UV-LED irradiation. AIP Conf Proc. 2020;2237(June).

3. Maaza M, Ngom BD, Achouri M, Manikandan K. Functional nanostructured oxides. Vacuum [Internet]. 2015;114:172–87. Available from: <URL>

4. Wellia DV, Kusumawati Y, Diguna LJ, Amal MI. Introduction of Nanomaterials for Photocatalysis. In: Khan MM, Pradhan D, Sohn Y, editors. Nanocomposites for Visible Light-induced Photocatalysis. Springer S. Springer, Cham; 2017. p. 1–17. Available from: <URL>

5. Mateo-Mateo C, Vázquez-Vázquez C, Pérez-Lorenzo M, Salgueiriño V, Correa-Duarte MA. Ostwald ripening of platinum nanoparticles confined in a carbon nanotube/silica-templated cylindrical space. J Nanomater. 2012;2012.

6. Villa A, Schiavoni M, Prati L. Material science for the support design: A powerful challenge for catalysis. Catal Sci Technol. 2012;2(4):673–82.

7. Morsbach E, Spéder J, Arenz M, Brauns E, Lang W, Kunz S, et al. Stabilizing catalytically active nanoparticles by ligand linking: Toward three-dimensional networks with high catalytic surface area. Langmuir. 2014;30(19):5564–73.

8. Villa A, Dimitratos N, Chan-Thaw CE, Hammond C, Veith GM, Wang D, et al. Characterisation of gold catalysts. Chem Soc Rev [Internet]. 2016;45(18):4953–94. Available from: <URL>

9. Campisi S, Schiavoni M, Chan-Thaw CE, Villa A. Untangling the role of the capping agent in nanocatalysis: Recent advances and perspectives. Catalysts. 2016;6(12):1–21.

10. Neouze MA, Schubert U. Surface modification and functionalization of metal and metal oxide nanoparticles by organic ligands. Monatshefte fur Chemie. 2008;139(3):183–95. Available from: <URL>

11. Javed R, Usman M, Tabassum S, Zia M. Effect of capping agents: Structural, optical and biological properties of ZnO nanoparticles. Appl Surf Sci [Internet]. 2016;386:319–26. Available from: <URL>

12. Ahmed S, Annu, Chaudhry SA, Ikram S. A review on biogenic synthesis of ZnO nanoparticles using plant extracts and microbes: A prospect towards green chemistry. J Photochem Photobiol B Biol. 2017;166:272–84. Available from: <URL>

13. Singh A, Singh NB, Hussain I, Singh H, Yadav V, Singh SC. Green synthesis of nano zinc oxide and evaluation of its impact on germination and metabolic activity of Solanum lycopersicum. J Biotechnol. 2016;233:84–94. Available from: <URL>

14. Zare M, Namratha K, Thakur MS, Byrappa K. Biocompatibility assessment and photocatalytic activity of bio-hydrothermal synthesis of ZnO nanoparticles by Thymus vulgaris leaf extract. Mater Res Bull. 2019;109(May 2018):49–59. Available from: <URL>

15. Putri OK, Syafdhanim H, Holilah, Fadlan A, Kusumawati Y, Santoso M, et al. Antioxidant and antibacterial activities of phytosynthesised ZnOs by hibiscus tiliaceus leaf extract against four pathogenic bacteria. Rasayan J Chem. 2022;15(4):2835–43.

16. Hosni M, Kusumawati Y, Farhat S, Jouini N, Pauporté T. Effects of oxide nanoparticle size and shape on electronic structure, charge transport, and recombination in dye-sensitized solar cell photoelectrodes. J Phys Chem C. 2014;118(30):16791–8.

17. Meshram J V., Koli VB, Phadatare MR, Pawar SH. Anti-microbial surfaces: An approach for deposition of ZnO nanoparticles on PVA-Gelatin composite film by screen printing technique. Mater Sci Eng C [Internet]. 2017;73:257–66. Available from: <URL>

18. Johnson MK, Powell DB, Cannon RD. Vibrational spectra of carboxylato complexes-I. Infrared and Raman spectra of beryllium(II) acetate and formate and of zinc(II) acetate and zinc(II) acetate dihydrate. Spectrochim Acta Part A Mol Spectrosc. 1981;37(10):899–904.

19. Anandan M, Dinesh S, Krishnakumar N, Balamurugan K. Improved photocatalytic properties and anti-bacterial activity of size reduced ZnO nanoparticles via PEG-assisted precipitation route. J Mater Sci Mater Electron. 2016;27(12):12517–26.

20. Nasrollahzadeh M, Issaabadi Z, Sajadi SM. Green synthesis of Pd/Fe3O4 nanocomposite using Hibiscus tiliaceus L. extract and its application for reductive catalysis of Cr(VI) and nitro compounds. Sep Purif Technol [Internet]. 2018;197(January):253–60. Available from: <URL>

21. Chen Z, Luo Y, Huang C, Shen X. In situ assembly of ZnO/graphene oxide on synthetic molecular receptors: Towards selective photoreduction of Cr(VI) via interfacial synergistic catalysis. Chem Eng J [Internet]. 2021;414(January):128914. Available from: <URL>

22. Aziz FFA, Jalil AA, Hassan NS, Hitam CNC, Rahman AFA, Fauzi AA. Enhanced visible-light driven multi-photoredox Cr(VI) and p-cresol by Si and Zr interplay in fibrous silica-zirconia. J Hazard Mater [Internet]. 2021;401(March 2020):123277. Available from: <URL>

23. Gawade V V., Sabale SR, Dhabbe RS, Kite S V., Garadkar KM. Bio-mediated synthesis of ZnO nanostructures for efficient photodegradation of methyl orange and methylene blue. J Mater Sci Mater Electron

[Internet]. 2021;32(24):28573–86. Available from: <URL>

24. Prasetyoko D, Sholeha NA, Subagyo R, Ulfa M, Bahruji H, Holilah H, et al. Mesoporous ZnO nanoparticles using gelatin — Pluronic F127 as a double colloidal system for methylene blue photodegradation. Korean J Chem Eng. 2023;40(1):112–23.

25. Subagyo R, Tehubijuluw H, Prasetyo Utomo W, Dwi Rizqi H, Kusumawati Y, Bahruji H, et al. Converting red mud wastes into mesoporous ZSM-5 decorated with TiO2 as an eco-friendly and efficient adsorbent-photocatalyst for dyes removal. Arab J Chem. 2022;15(5):103754. Available from: <URL>

26. Azami MS, Jalil AA, Hassan NS, Hussain I, Fauzi AA, Aziz MAA. Green carbonaceous material–fibrous silica-titania composite photocatalysts for enhanced degradation of toxic 2-chlorophenol. J Hazard Mater [Internet]. 2021;414(December 2020):125524. Available from: <URL>

27. Zulfa LL, Ediati R, Hidayat ARP, Subagyo R, Faaizatunnisa N, Kusumawati Y, et al. Synergistic effect of modified pore and heterojunction of MOF-derived α-Fe2O3/ZnO for superior photocatalytic degradation of methylene blue. RSC Adv. 2023;13(6):3818–34.

28. Lam SM, Jaffari ZH, Sin JC, Zeng H, Lin H, Li H, et al. Surface decorated coral-like magnetic BiFeO3 with Au nanoparticles for effective sunlight photodegradation of 2,4-D and E. coli inactivation. J Mol Liq. 2021;326:115372. Available from: <URL>

29. Yong ZJ, Lam SM, Sin JC, Zeng H, Mohamed AR, Jaffari ZH. Boosting sunlight-powered photocatalytic fuel cell with S-scheme Bi2WO6/ZnO nanorod array composite photoanode. Inorg Chem Commun. 2022;143(August):109826. Available from: <URL>

30. Subagyo R, Yudhowijoyo A, Sholeha NA, Hutagalung SS, Prasetyoko D, Birowosuto MD, et al. Recent advances of modification effect in Co3O4-based catalyst towards highly efficient photocatalysis. J Colloid Interface Sci. 2023;650(PB):1550–90. Available from: <URL>